

*Annual Review of Analytical Chemistry*

# Electrochemical Imaging of Interfaces in Energy Storage via Scanning Probe Methods: Techniques, Applications, and Prospects

Abhiroop Mishra, Dipobrato Sarbapalli,  
Oliver Rodríguez, and Joaquín Rodríguez-López

Department of Chemistry, University of Illinois Urbana-Champaign, Urbana, Illinois, USA;  
email: joaquinr@illinois.edu

Annu. Rev. Anal. Chem. 2023. 16:93–115

First published as a Review in Advance on  
April 17, 2023

The *Annual Review of Analytical Chemistry* is online at  
anchem.annualreviews.org

<https://doi.org/10.1146/annurev-anchem-091422-110703>

Copyright © 2023 by the author(s). This work is licensed under a Creative Commons Attribution 4.0 International License, which permits unrestricted use, distribution, and reproduction in any medium, provided the original author and source are credited. See credit lines of images or other third-party material in this article for license information.

ANNUAL  
REVIEWS **CONNECT**

[www.annualreviews.org](http://www.annualreviews.org)

- Download figures
- Navigate cited references
- Keyword search
- Explore related articles
- Share via email or social media

## Keywords

AFM, automation, batteries, deep learning, interface, imaging, SECCM, SECM, SICM

## Abstract

Developing a deeper understanding of dynamic chemical, electronic, and morphological changes at interfaces is key to solving practical issues in electrochemical energy storage systems (EESSs). To unravel this complexity, an assortment of tools with distinct capabilities and spatiotemporal resolutions have been used to creatively visualize interfacial processes as they occur. This review highlights how electrochemical scanning probe techniques (ESPTs) such as electrochemical atomic force microscopy, scanning electrochemical microscopy, scanning ion conductance microscopy, and scanning electrochemical cell microscopy are uniquely positioned to address these challenges in EESSs. We describe the operating principles of ESPTs, focusing on the inspection of interfacial structure and chemical processes involved in Li-ion batteries and beyond. We discuss current examples, performance limitations, and complementary ESPTs. Finally, we discuss prospects for imaging improvements and deep learning for automation. We foresee that ESPTs will play an enabling role in advancing EESSs as we transition to renewable energies.

Downloaded from [www.annualreviews.org](http://www.annualreviews.org).

Guest (guest)

IP: 18.223.118.70

93

On: Thu, 16 May 2024 16:04:41

## 1. INTRODUCTION

**Anode:** in battery terminology, the anode is the negative electrode, i.e., where oxidation takes place during the discharge process

**Cathode:** in battery terminology, the cathode is the positive electrode, i.e., where reduction takes place during the discharge process

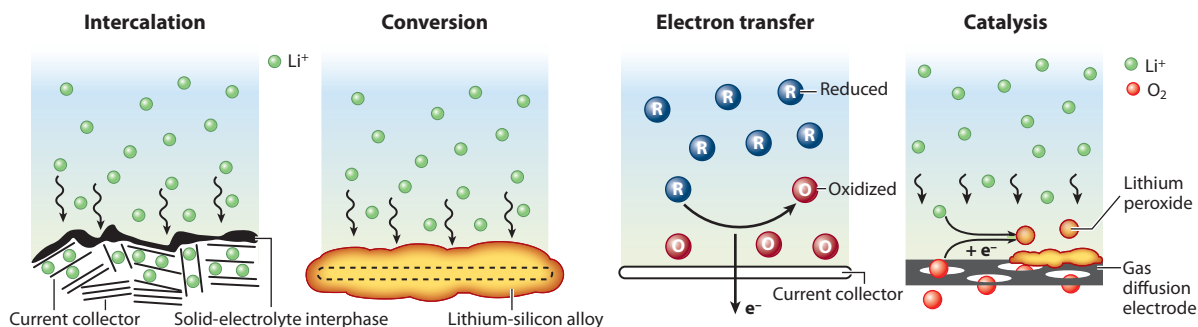
**Intercalation:** reversible insertion of an external species into a host without causing significant distortion in the host's crystal structure

**Conversion:** a reversible reaction leading to the formation of an alloy, such as Li alloying with Si, Sn, Al, etc.

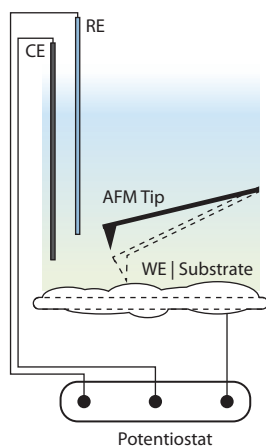
Electrochemical energy storage systems (EESSs) are central to portable electronics, transport electrification, and the future of the electrical grid (1, 2). The pressing need to transition from fossil fuels to renewable energy technologies necessitates improving the existing EESSs, such as Li-ion batteries (LiBs), and developing novel battery chemistries beyond Li (1). While there are numerous material developments for anodes, cathodes, and separators for batteries, integrating them into practical devices, and characterizing them within, is often a challenge. A primary reason is that battery components are sealed in inert atmospheres, in the absence of water and oxygen, preventing conventional approaches for their characterization. In addition, battery operation requires the prior formation of interphases, *in situ*. For example, the formation step in LiB production chains involves parasitic reactions with electrolytes to form interphases on the anode, which largely influences battery performance and safety (3). While highly informative, techniques such as electron microscopy and X-ray photoelectron spectroscopy utilized for interface characterization in EESSs suffer due to their *ex situ* nature. Their main drawbacks include sample damage caused by energetic beams, the need for high vacuum, and complex sample preparation, for example, thinning or the need for single crystals (4). In this regard, electrochemical scanning probe techniques (ESPTs) are uniquely positioned to circumvent these issues. These tools are interface sensitive by nature and enable high spatiotemporal resolution for the investigation of interfacial processes in realistic battery environments.

Highly localized variations of charge transport properties at interfaces versus the bulk, such as electronic and ionic conductivity, can control the performance of an entire battery. This calls for using an assortment of tools that are capable of measuring processes involving ionic and electronic transport, redox reactivity, and chemical evolution with interfacial sensitivity, ideally with high spatial and temporal resolutions. ESPTs are well positioned to address these needs since they offer versatile modes and approaches to characterize different localized interfacial processes. **Figure 1a** shows some of the common interfacial processes in batteries such as intercalation, conversion, electron transfer, and catalysis. This review highlights four popular ESPTs that are used for mechanistic exploration of battery interfaces: scanning electrochemical microscopy (SECM), scanning ion conductance microscopy (SICM), scanning electrochemical cell microscopy (SECCM), and electrochemical atomic force microscopy (EC-AFM), as illustrated in **Figure 1b–e** with their distinct electrochemical components (see the sidebar titled Basic Electrochemical Terms). SECM, SECCM, and SICM can provide a diverse range of information ranging from electrochemical reactivity to topography of interfaces and interphases. Similarly, EC-AFM provides the capability to probe the morphological and mechanical characteristics of these structures. A key feature of these measurements is that they are typically nondestructive, enabling measurements to be free of artifacts such as beam damage that may arise in electron microscopy approaches. In addition, comprehensive chemical, morphological, and electrochemical characterization can be performed via correlative experiments, or by coupling spectroscopy- (5–7) or X-ray- (8, 9) based measurements to ESPTs. The interested reader is referred to previous reviews covering analytical methods for EESSs (10), including nanoscale electrochemistry (11, 12) and focused reviews covering the application of an individual ESPT (13, 14). The scope of this review is limited to recent *in situ* and *operando* studies utilizing these ESPTs on LiBs and other novel battery chemistries beyond Li ion. Section 2 provides a brief background on each ESPT, followed by Sections 3 and 4 covering applications of ESPTs to LiBs and beyond-Li battery chemistries, respectively. Section 5 provides a critical outlook of the crossroads between ESPTs and emerging computational tools for materials research.

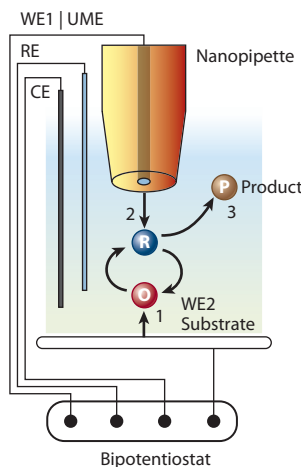
**a** Common types of energy storage processes with examples



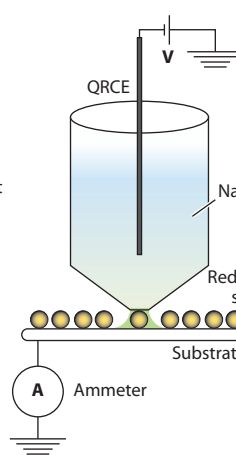
**b** Electrochemical atomic force microscopy



**c** Scanning electrochemical microscopy



**d** Scanning electrochemical cell microscopy



**e** Scanning ion conductance microscopy

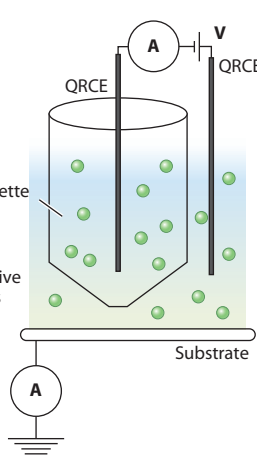


**Figure 1**

Scheme of different battery processes and ESPTs covered in this review. (a) Energy storage processes in different battery chemistries, including intercalation, conversion, electron transfer, and catalysis. (b–e) Typical setup of four popular ESPTs: (b) electrochemical AFM; (c) scanning electrochemical microscopy, with arrow 1 representing substrate generation, arrow 2 representing tip collection, and arrow 3 representing the product diffusing away; (d) scanning electrochemical cell microscopy; and (e) scanning ion conductance microscopy. Abbreviations: AFM, atomic force microscopy; CE, counter electrode; ESPT, electrochemical scanning probe technique; QRCE, quasi-reference counter electrode; RE, reference electrode; UME, ultramicroelectrode; WE, working electrode.

## 2. A PRIMER ON ESPTs APPLIED TO EESSs

During battery operation, several processes simultaneously take place at the electrode–electrolyte interface such as solvent breakdown, interphase formation, and ion intercalation (15). These lead to changes in morphological, mechanical, electrical, and electrochemical properties of the electrodes. ESPTs utilize local physical or electrochemical interactions between a small probe (or tip) and the sample (or substrate) enabling micro- to nanoscale investigations of the changes in these properties. For further details regarding in-depth working principles of these ESPTs, we direct readers to additional literature on EC-AFM (14), SECM (13, 16), SECCM (17–19), and SICM (20, 21) (see the sidebar titled ESPTs).

## BASIC ELECTROCHEMICAL TERMS

- Probe/tip: an element such as a nanopipette, cantilever tip, or an ultramicroelectrode that measures a local property when positioned above the substrate.
- Working electrode (WE): electrode on which experimental processes are monitored and analyzed; in potentiostatic experiments, the potential of this electrode is controlled.
- Counter electrode: typically, a large-area electrode that passes current without limiting electrochemical process rates at the WE.
- Reference electrode: an electrode with a constant potential, often governed by the Nernst equation, i.e., a poised system, that serves as a reference to control the potential of the WE; a quasi-reference electrode on the other hand presents a sufficiently constant potential to be practical but may be unpoised.
- Bipotentiostat: an instrument capable of controlling the potential of two electrodes distinctly and simultaneously using a common reference and counter electrode.
- Cyclic voltammetry: an electrochemical measurement where the potential of a WE is scanned with respect to time in a linear fashion between two chosen potential limits, i.e., at a constant scan rate with forward and backward scan sweeps, while simultaneously recording the current at the WE.

## ESPTs

- EC-AFM: scanning probe microscopy that uses cantilever probes and mechanically interacts with surface forces; specifically for EC-AFM, these tips operate under liquid electrolyte measuring forces and electrical phenomena while the substrate performs electrochemical measurements.
- SECM: an electrochemical scanning probe technique (ESPT) using an ultramicroelectrode/nanoelectrode as the probe; SECM can quantify and map electron-transfer kinetics between a redox mediator and a substrate, and it can also be used to electrochemically investigate species generated from the substrate.
- SECCM: an ESPT using a micropipette/nanopipette that forms an electrochemical cell by encapsulating a small region of the substrate in a droplet meniscus; it can be used to obtain spatially resolved electrochemical properties without the contribution of other areas on the substrate.
- SICM: an ESPT using a micropipette/nanopipette that can be used to track changes in topography or local ionic concentrations by measuring ionic resistance between two quasi-reference counter electrodes, at least one of which is placed inside a pipette.

### 2.1. Electrochemical Atomic Force Microscopy

EC-AFM, similar to typical AFM measurements, relies on the local physical interactions between a small cantilever tip and the sample surface (**Figure 1b**) to map local mechanical and electrical properties. However, these measurements are performed in situ within a liquid environment incorporating a reference and a counter electrode leading to the formation of an electrochemical cell. In the domain of EESSs, the instrument is usually placed inside an argon-filled glovebox to prevent exposing the samples to oxygen and moisture. EC-AFM has been used in a wide range of applications ranging from morphological investigation of interphases on commercial materials (22–24) to studying volume changes in the next-generation electrode materials in EESSs (25, 26).

## 2.2. Scanning Electrochemical Microscopy

A typical SECM setup consists of a probe, often an inlaid-disc ultramicroelectrode (UME) tip (diameter  $\leq 25 \mu\text{m}$ ) (27), that is positioned close to a substrate for interrogating local electrochemical properties. Feedback imaging (depicted by arrows 1 and 2 in the SECM schematic in **Figure 1c**) is performed by measuring the tip current resulting from the electrolysis of a redox mediator while the UME is rastered across the substrate and biased to attempt redox regeneration of the mediator. Feedback imaging provides a way to map and visualize electrochemically active and inactive regions on the substrate. In practice, this enables in situ investigation of passivating processes, for example, interphase formation in LiBs. Other modes such as substrate generation/tip collection illustrated in **Figure 1c** are used to study battery degradation by detecting the products. For example, oxygen released from a decomposing LiB cathode (substrate generation step; arrow 1 in **Figure 1c**) can be detected at the tip using oxygen reduction reaction (tip collection step; arrow 2 in **Figure 1c**). The resulting products from the tip collection step can either diffuse away (arrow 3 in **Figure 1c**) or become part of a feedback loop if they are redox-active (28). The unique capabilities of SECM allow investigation of two fundamental processes driving EESSs: ion and electron transfer (ET) processes at an interface (13).

---

**Redox mediator:** species capable of undergoing oxidation/reduction reactions with a desired structure with the purpose of exchanging charge between them

---

## 2.3. Scanning Electrochemical Cell Microscopy

SECCM is a micro-/nanopipette-based ESPT that enables the characterization of local electrochemical behavior by isolating a substrate area within a droplet meniscus, as shown in **Figure 1d** (17). A simple SECCM setup utilizes a single pipette, with the substrate being a conducting working electrode (WE) and a combined quasi-reference counter electrode (QRCE) placed inside the pipette (17). Typically, measurements are performed by applying a potential to the QRCE while measuring the current from the WE. Imaging is performed by a hopping protocol where the tip is retracted and approached over different locations. A dual-barreled pipette can be used with the same protocol but also facilitates imaging via rastering, with positioning feedback collected from changes in ionic current between the QRCEs in each barrel (18). SECCM with such a pipette enables the simultaneous measurement of local electrochemical activity and topographical features of conducting and insulating substrates (17, 19).

## 2.4. Scanning Ion Conductance Microscopy

SICM is another micro-/nanopipette-based technique developed by Hansma et al. (29) for generating topographic and ionic conductivity maps of substrates. It tracks local ionic currents between QRCEs inside the pipette and in bulk solution upon application of a potential bias, as depicted in **Figure 1e**. Feedback signals are obtained from the change in ionic resistance as the tip is brought closer to the surface (20, 29, 30). A key advantage of SICM is its ability to obtain measurements without the use of redox mediators. With these strengths, SICM has been used to study topographical changes (31–33) and ionic fluxes (32) in situ on operating battery electrodes. In other applications, SICM has been utilized to study ionic conductivity through membranes (34) and porous battery cathodes (35), which are also active research areas in the domain of EESSs.

## 3. APPLICATION OF ESPTs FOR IN SITU INVESTIGATION OF LI-ION BATTERIES

LiBs typically consist of host electrode materials that can reversibly (de)intercalate Li ions during battery operation, as shown in **Figure 1a**. The electrode-electrolyte interface is a dynamic region where multiple processes occur simultaneously, thereby making their investigation a challenge.

## INTERFACE VERSUS INTERPHASE

Interphases and interfaces are not the same. While an interface refers to the location where two dissimilar media meet, an interphase refers to a separate phase that forms at an interface. For example, the solid-electrolyte interphase, a structure that has distinct chemical and mechanical properties, forms over the anode due to reactions at the anode-electrolyte interface during Li-ion battery operation.

These processes include interphase formation (36) and loss of active materials (37, 38). Below, we discuss how ESPTs have been utilized for the in situ investigation of these processes, thereby developing a comprehensive understanding of the dynamic interfaces.

### 3.1. Li-Ion Battery Anode Materials

Commercial LiB anodes are typically composed of graphite (39) which functions as an intercalation host for Li ions. These anodes operate beyond the thermodynamic stability window of the electrolyte solution, leading to electrolyte decomposition and the formation of a solid-electrolyte interphase (SEI) (36) (see the sidebar titled Interface Versus Interphase). The SEI film is crucial in controlling the performance of the LiB since it must be electronically insulating to prevent further electrolyte decomposition and ionically conducting to enable Li-ion (de)intercalation. SEI formation also occurs on Li metal and on advanced anode materials such as silicon, which forms an alloy with Li. Silicon and Li-metal anodes are also subject to significant volume changes during cycling (40), making it essential to characterize their deformation in situ. Consequently, the mechanical properties of the SEI become crucial since it must resist fracture during volume changes. As shown below, ESPTs can be used to study these relevant processes, such as the SEI's mechanical and electrical properties and tracking the electrodes' deformation.

**3.1.1. Passivation by solid electrolyte interphase.** The critical role of the SEI lies in preventing continuous electrolyte decomposition; therefore, its electronic passivating properties are of significant importance. In this regard, SECM in the feedback mode has been utilized extensively to study the SEI passivation using redox mediators such as ferrocene. After SEI formation, the anode behavior transitions from electronically conducting to insulating. This leads to a drop in the feedback current measured at the SECM tip and provides real-time information about SEI properties. Using this principle, several studies reported the SEI formation dynamics on a variety of materials such as graphite (41, 42), highly oriented pyrolytic graphite (HOPG) (43), multilayer graphene (44), and TiO<sub>2</sub> (45) by repeated imaging of the same region during electrochemical cycling. Similarly, SECM has been applied to optimize preprocessing conditions influencing SEI formation on silicon anode materials such as silicon clathrates (46). These applications illustrate the use of SECM to characterize existing and next-generation anodes for LiBs.

While SECM has enabled the detection of passivation due to SEI formation, higher spatial resolution is required to correlate the way surface structural features influence this process. To this end, Unwin and coworkers (47) used SECCM to correlate the effects of carbon electrode structure on SEI formation. Their study utilized commercially relevant electrolytes with HOPG substrates using hopping-mode SECCM (**Figure 2a**). Voltammetric measurements were performed with SECCM leading to SEI formation, as depicted in **Figure 2b**. The HOPG substrates possessed varying structural features, observed via AFM, as shown in **Figure 2c**. These structural features were correlated to passivation, as quantified by the ratio of irreversible charge passed to form the SEI from two cyclic voltammetry cycles ( $Q_{p2}/Q_{p1}$ ; **Figure 2d**) at approximately 1,000 spots. A

**HOPG:** a graphitic carbon characterized by its crystallinity, flatness, and ease of preparation of freshly cleaved clean surfaces

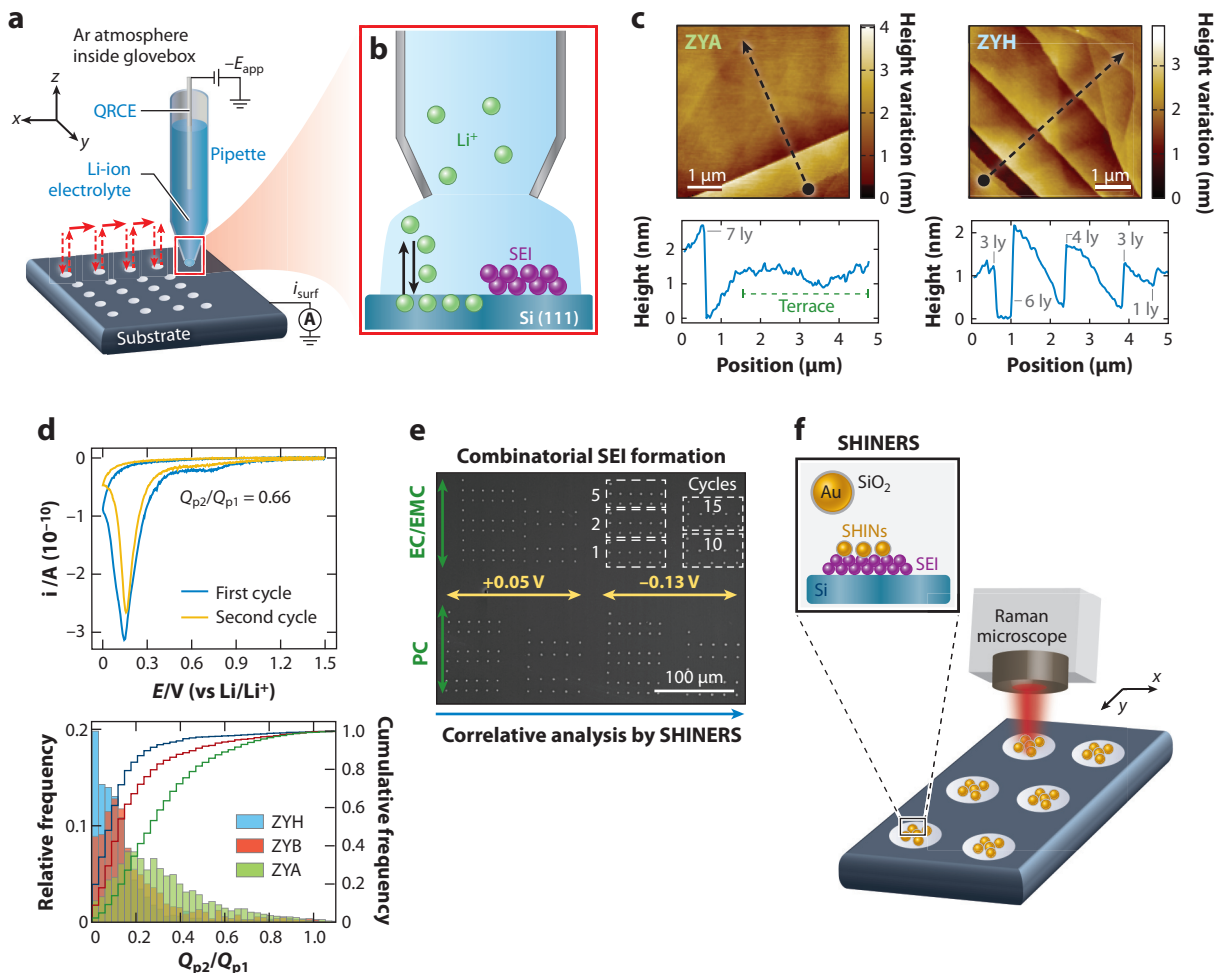


**Figure 2**

Application of SECCM to study SEI formation. (a) Scheme of SECCM hopping mode implemented inside an Ar-filled glovebox for extracting localized information such as (b) SEI formation on anodes. (c) AFM characterization of HOPG anodes used in the study revealed differences in edge plane densities. The black dot is the starting point (0 μm) and the arrow is the direction where distance is increasing. This refers to the height variation plot below. (d) Characterization of passivation using two CV cycles and measuring the ratio of charge passed ( $Q_{p2}/Q_{p1}$ ) followed by cluster analysis of this parameter over multiple spots. (e) Measurement protocol illustrating how SECCM can be used to explore combinatorial parameters such as potential window, scan rate, and number of scans, e.g., on SEI formation. (f) Illustration of SECCM combinatorial measurements coupled to colocalized Raman using SHINERS. Abbreviations: AFM, atomic force microscopy; CV, cyclic voltammetry;  $E_{\text{app}}$ , potential applied; EC, ethylene carbonate; EMC, ethyl methyl carbonate; HOPG, highly oriented pyrolytic graphite;  $i_{\text{surf}}$ , the current at the substrate; PC, propylene carbonate; SECCM, scanning electrochemical cell microscopy; SEI, solid-electrolyte interphase; SHINs, shell-isolated nanoparticles; SHINERS, shell-isolated nanoparticles for enhanced Raman spectroscopy. Panels a, b, e, and f adapted with permission from Reference 48. Panels c and d adapted with permission from Reference 47; copyright 2021 Wiley-VCH.

cluster analysis of these values showed that the highest amount of passivation was attributed to HOPG substrates with the highest density of edge planes. In summary, this work illustrates the value of in situ SECCM analysis on precharacterized substrates, resulting in an understanding of structure-SEI formation correlations.

Downloaded from www.annualreviews.org.

Guest (guest)

www.annualreviews.org • Imaging of Interfaces in Energy Storage 99

On: Thu, 16 May 2024 16:04:41

The high versatility of SECCM to perform a high number of spot measurements on an electrode was also used for the combinatorial analysis of operating conditions influencing SEI formation (48). For example, SEI formation and its properties are influenced by parameters such as scan rate, number of scans, potential window, choice of electrolyte, and so on. SECCM investigation of these parameters over a silicon anode is shown in **Figure 2e**. These experiments involved multiple repeats for each parameter investigated, enabling statistical comparisons. The total duration for the entire experiment was only 2 h, which highlights the ability of SECCM as a powerful combinatorial tool for high-throughput analysis in battery research. This experiment also highlights the benefits of using ESPTs for correlative analysis. The ability to locate spots by the electrolyte footprint left after SECCM measurements was subsequently exploited to perform colocalized characterization by shell-isolated nanoparticles for enhanced Raman spectroscopy (SHINERS). Au-SiO<sub>2</sub> shell isolated particles were deposited on the silicon substrate after SECCM measurements, leading to chemical characterization of SEI properties using Raman spectroscopy (48) (**Figure 2f**). Correlating Raman spectra with SECCM data identified an initial decrease in the decomposition rate of LiPF<sub>6</sub> salt; however, this process reactivated after multiple cycles. This observation indicated that either the SEI formation processes were reversible or some instabilities led to pristine silicon surfaces being exposed for further decomposition reactions. Such information can be promising in studying mechanistic aspects of SEI formation on various materials, along with choosing formation cycling protocols for practical LiBs.

### 3.1.2. Mechanical and morphological characterization of the solid-electrolyte interphase.

The morphological evolution of SEI films and their corresponding mechanical properties can be probed through EC-AFM. For example, the SEI was revealed to grow in thickness beyond the first (dis)charge cycle on materials such as graphite and HOPG (49–52). These observations contrasted with the general perception that an unchanging SEI forms rapidly (53). Additionally, EC-AFM revealed differences in SEI homogeneity, with thicker SEIs observed on graphite edge planes compared to basal planes (54, 55). This is consistent with the fact that Li-ion intercalation only occurs through edge planes (42, 56).

In probing the effects of electrode structure on resulting SEIs, in situ EC-AFM measurements compared SEI formation on HOPG and industry-relevant graphite materials (22). Graphite particles were observed to possess a greater coverage of SEI and had a lower Young's modulus compared to SEIs on HOPG. This finding is critical when correlating the fundamental SEI studies performed on HOPG to the device-level performance of graphite-based batteries. Regarding varying electrolyte solutions, Shen et al. (57) reported that fluorinated electrolytes facilitated the formation of a harder and denser SEI (~1,498 MPa) as compared to traditional carbonate electrolytes (~916 MPa), thereby leading to more stable interphases. EC-AFM along with impedance measurements were also used in the identification of operating conditions where a favorable SEI was formed; at higher operating potentials, softer SEIs with lower ionic conductivity were found at the electrode surface. On the other hand, lower potentials led to a SEI with higher elastic moduli and more inorganic components (58). Combining in situ EC-AFM with other characterization tools has allowed a more detailed investigation of SEI formation mechanisms. For example, comparing electrochemical quartz crystal microbalance data with morphological changes by EC-AFM revealed the multiple stages of SEI formation (24). **Figure 3a,b** illustrates two of these stages during the first lithiation cycle of HOPG at 0.74 V and 0.6 V versus Li<sup>+</sup>/Li, respectively. As interlayer sites become continuously populated with Li ions, the interlayer spacing increases. A sharp increase was observed below 0.6 V, as shown in **Figure 3b**, due to the onset of ethylene carbonate reduction, leading to the generation of both gaseous and organic Li-salt products. **Figure 3c,d** represents the topographical images of HOPG while performing

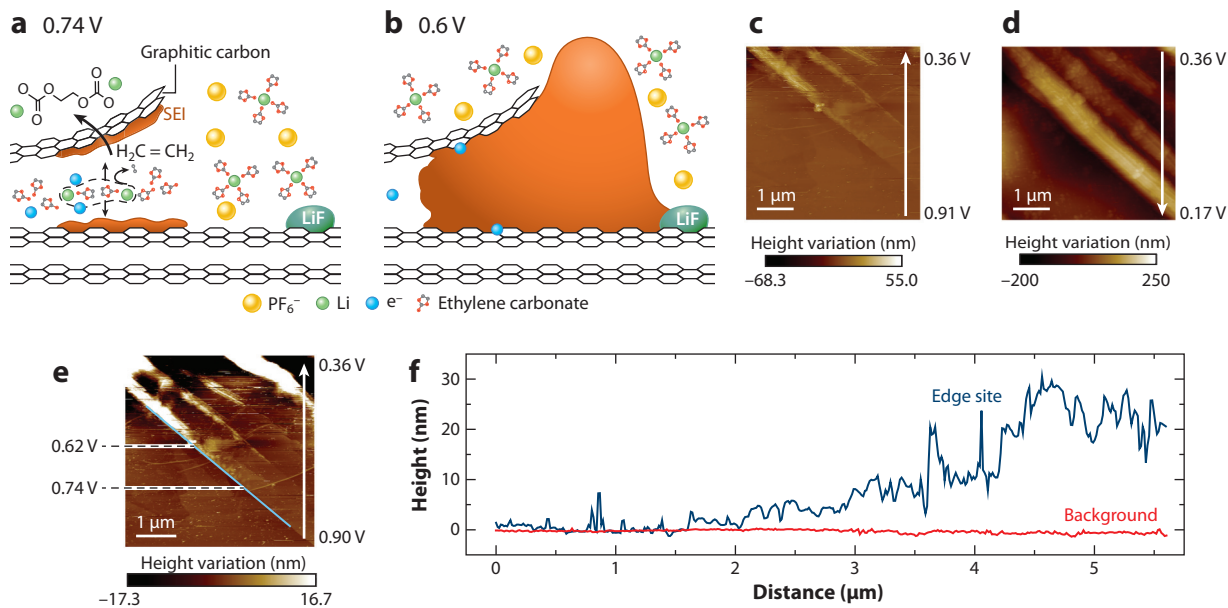


**Figure 3**

In situ electrochemical atomic force microscopy (EC-AFM) for investigating solid-electrolyte interphase (SEI) formation on highly oriented pyrolytic graphite (HOPG). Schematic shows interphase formation during the first lithiation cycle at (a) 0.74 V and (b) 0.6 V. (c,d) Topographical images during cyclic voltammetry at HOPG. White arrows indicate scan directions. (e) Morphology and potential correlation during the initial scan from 0.90 V to 0.36 V, where the blue line shows the direction of the edge site. (f) SEI height variation (blue curve) is shown for the blue-labeled edge site in panel e and the background (red curve). All potentials are described versus a  $\text{Li}^+/\text{Li}$  reference scale. Figure adapted with permission from Reference 24; copyright 2019 Springer Nature.

voltammograms at the substrate. The SEI on the labeled edge site in **Figure 3e** was found to increase in height as shown in **Figure 3f** when the applied potential on HOPG decreased from 0.9 V to 0.36 V versus  $\text{Li}^+/\text{Li}$ . In summary, these measurements reveal the strengths of applying EC-AFM to extract mechanistic, morphological, and mechanical information on SEI formation.

**3.1.3. Tracking deformation on operating Li-ion battery anodes.** In addition to tracking changes in morphology, EC-AFM has also been widely utilized to study volumetric changes in anode materials during LiB operation. For example, in situ EC-AFM was used to study the impact of silicon crystallinity on volume expansion, with polycrystalline silicon showing greater volume changes as compared to amorphous silicon during electrochemical cycling (59). Later, the degree of volume change in amorphous cylindrical silicon samples was shown to depend on their initial size (diameter and height). This study helped in developing a design strategy of having smaller-sized silicon anodes for achieving lower volumetric changes (60).

In addition to silicon, there is active interest in implementing Li metal as anodes. However, Li metal suffers from severe volumetric changes and dendrite formation during operation (40). To address these problems, Shen et al. (26) employed EC-AFM to characterize the effects of a novel graphite-LiF-based artificial coating, which was found to prevent dendrite formation, therefore enabling Li-metal-based batteries with long cycle life. Krueger et al. (61) used SECM for probing the Li-anode interfacial reactivity changes as a function of galvanostatic cycling conditions on these interfaces. A key finding from their study was identifying high ET rates over areas prone to dendrite formation, relative to the rest of the sample. Such studies could be extended to other

**Galvanostatic cycling:** the process of controlling a current imposed on a working electrode while recording its potential

---

**Potentiostatic**

**cycling:** the process of controlling the potential of a working electrode while recording the current it passes

---

electrolytes and operating conditions to develop strategies to minimize dendrite formation in Li-metal anodes.

**3.1.4. Ionic flux measurements.** SICM has also been used to track deformation occurring in hard carbon and HOPG anode materials, but use of a dual barreled tip adds the capability to measure local electrolyte concentrations and ionic fluxes (32). Using the sensitivity offered by tracking ionic resistance close to the pipette, it was possible to characterize topography and deformation in situ to the nanometer level. A simple calibration curve enabled the correlation of ionic currents to electrolyte concentrations in the vicinity of the tip. Subsequently, SICM was used to measure the local electrolyte fluxes through changes in ionic currents. Interestingly, the ionic current increased during Li-ion intercalation, which indicated that the concentration of electrolytes near the carbon substrate was higher than the bulk concentration. These results suggest that the SICM ionic current measurement may be carrying contributions from anion migration or other transport processes. Although performed at different electrolyte concentrations, the SICM experiment contrasts with flux measurements obtained with ion-sensitive SECM using Hg UME tips over HOPG (62, 63). Hg UMEs, which selectively detect Li ions, revealed a sharp decrease in their local concentration upon intercalation and a corresponding increase upon deintercalation. Nonetheless, SICM imaging measurements clearly show changes in the ionic response exhibited at much higher spatial resolution during topography imaging owing to the small pipette size, compared to those achievable by ion-sensitive SECM measurements (62). Interestingly, the SECM approach also showed significant ion fluxes in the SEI formation potential window, suggesting reversible ion exchange in an active SEI. Using ESPTs for performing ion flux measurements is an open frontier, especially in the domain of LiBs and technologies using alternative ions such as  $\text{Na}^+$  and  $\text{K}^+$  (64).

## 3.2. Li-Ion Battery Cathode Materials

There are three common classes of transition metal oxides that are typically used as cathodes in LiBs: layered, spinel, and polyanion oxides (65). During charging, Li ions delithiate from the cathodes and intercalate within graphitic anodes. At high states of delithiation, degradation processes such as loss of active material and solvent breakdown occur at the cathode, subsequently leading to cathode-electrolyte interphase (CEI) formation. The elucidation of these processes remains an ongoing pursuit with practical implications. Their investigation is even more challenging in commercial composite cathodes, which have spatial heterogeneity in active material, binder, and conductive carbon distribution (66).

**3.2.1. Heterogeneity in cathode materials.** Typical composite cathodes in LiBs have a heterogeneous microstructure that results in different sites having different chemical and electrochemical activity (66). There arises a need to elucidate these differences to better understand processes such as rate of ion (de)lithiation and interphase formation on different sites on the cathode. SECCM offers unique capabilities to characterize local activity of single particles, as reported through hopping mode measurements on  $\text{LiFePO}_4$  (LFP) cathodes (67). The hopping protocol enabled simultaneous identification of topographical features and electrochemical behavior of a single LFP particle. Subsequent correlations were made with scanning electron microscopy (SEM) and energy-dispersive spectroscopy to unambiguously identify active LFP and carbon black. Other submicron-resolution SECCM measurements have also been reported on active materials such as  $\text{Li}_4\text{Ti}_5\text{O}_{12}$  anode films (68), LFP single particles/films (67–69),  $\text{LiMn}_2\text{O}_4$  (LMO) particles (70), and  $\text{ZrO}_2$ -coated cathodes (71). In several of these applications, potentiostatic and galvanostatic cycling with SECCM was utilized to check for particle-to-particle or film heterogeneity (69–71).

Downloaded from www.annualreviews.org.

Guest (guest)

IP: 18.223.118.70

On: Thu, 16 May 2024 16:04:41

Complementary information on electrical properties can also be obtained from EC-AFM, with studies reporting sufficiently high resolution to identify variations in electrical properties within a single particle (72).

**3.2.2. Cathode material degradation processes.** A key challenge in LiBs is the lattice oxygen loss from cathodes at high operating potentials (37, 73). In a recent study, SECM was used for the real-time, quantitative detection of oxygen evolution from three commercial LiB cathodes: LiCoO<sub>2</sub> (LCO), LiNi<sub>0.33</sub>Mn<sub>0.33</sub>Co<sub>0.33</sub>O<sub>2</sub> (NMC111), and LiNi<sub>0.8</sub>Mn<sub>0.1</sub>Co<sub>0.1</sub>O<sub>2</sub> (NMC811) (28). **Figure 4a** shows the schematic of the measurement where a 25- $\mu$ m Au UME was placed close to the cathode surface while potentiostatically charging the latter. Lattice oxygen release was detected at the UME via the oxygen reduction reaction (ORR), thereby leading to a rise in UME current. **Figure 4b,c** shows the oxygen evolution from NMC111 and NMC811, respectively, as a function of applied cathode potential. The high sensitivity of this method led to the detection of an incipient oxygen evolution process around 3 V versus Li<sup>+</sup>/Li, which was unreported in the literature. In addition, the spatial resolution of SECM captured the heterogeneity in the oxygen evolution process through mapping experiments, as shown in **Figure 4d**. This method overcame the limitations of differential electrochemical mass spectrometry, the most widely used technique to study gas evolution in LiBs (74–76), such as low signal-to-noise ratio and lack of spatial resolution. Lattice oxygen loss is a critical phenomenon since it is known to be associated with surface reconstruction processes, which are known to be deleterious during prolonged battery cycling (77). Therefore, fast and sensitive identification of oxygen loss via SECM provides a promising direction in developing a better understanding of such transient processes. In addition, the versatility of SECM also enabled the investigation of Mn dissolution from LMO cathodes, which is another critical degradation process (38, 78). SECM can play a critical role in identifying mitigation approaches such as cathode compositions and artificial coatings, which may lead to the development of materials resistant to such degradation processes.

**3.2.3. Cathode-electrolyte interphase formation and stability.** The CEI has been reported to be an order of magnitude thinner than the SEI formed on anodes, and thus its characterization results in more challenging experiments (79). EC-AFM, however, helped in the visualization of the CEI and its effect on the capacity retention in LiBs. One such study illustrated the CEI formation on LCO with and without an artificial Al<sub>2</sub>O<sub>3</sub> coating (80). These measurements illustrated differences in morphology of the resulting CEIs, which were also linked to an improvement in capacity retention during battery cycling. Additionally, these imaging measurements highlighted that CEI is selectively formed on LCO edge planes, which is also the site for Li-ion intercalation. Contrary to interphases on anodes, which are insulating in nature (36) and therefore prevent continuous electrolyte decomposition, in situ SECM feedback measurements reported CEIs on LMO, NMC111, and LiNi<sub>0.5</sub>Mn<sub>1.5</sub>O<sub>4</sub> to be at least partially electronically conducting (81, 82). These examples illustrate how EC-AFM and SECM may be utilized to study CEIs formed on engineered cathode materials with artificial coatings for better device performance.

### 3.3. Outlook on ESPTs in the Domain of Li-Ion Batteries

A major challenge associated with ESPT usage is operating it in a glovebox, with relevant electrolytes used in commercial LiBs such as 1-M LiPF<sub>6</sub> in volatile carbonate solvent mixtures, for example, ethylene carbonate–diethyl carbonate (15). Since ESPTs necessitate the use of open cells to enable scanning, most research on batteries has been carried out in solvents such as aqueous

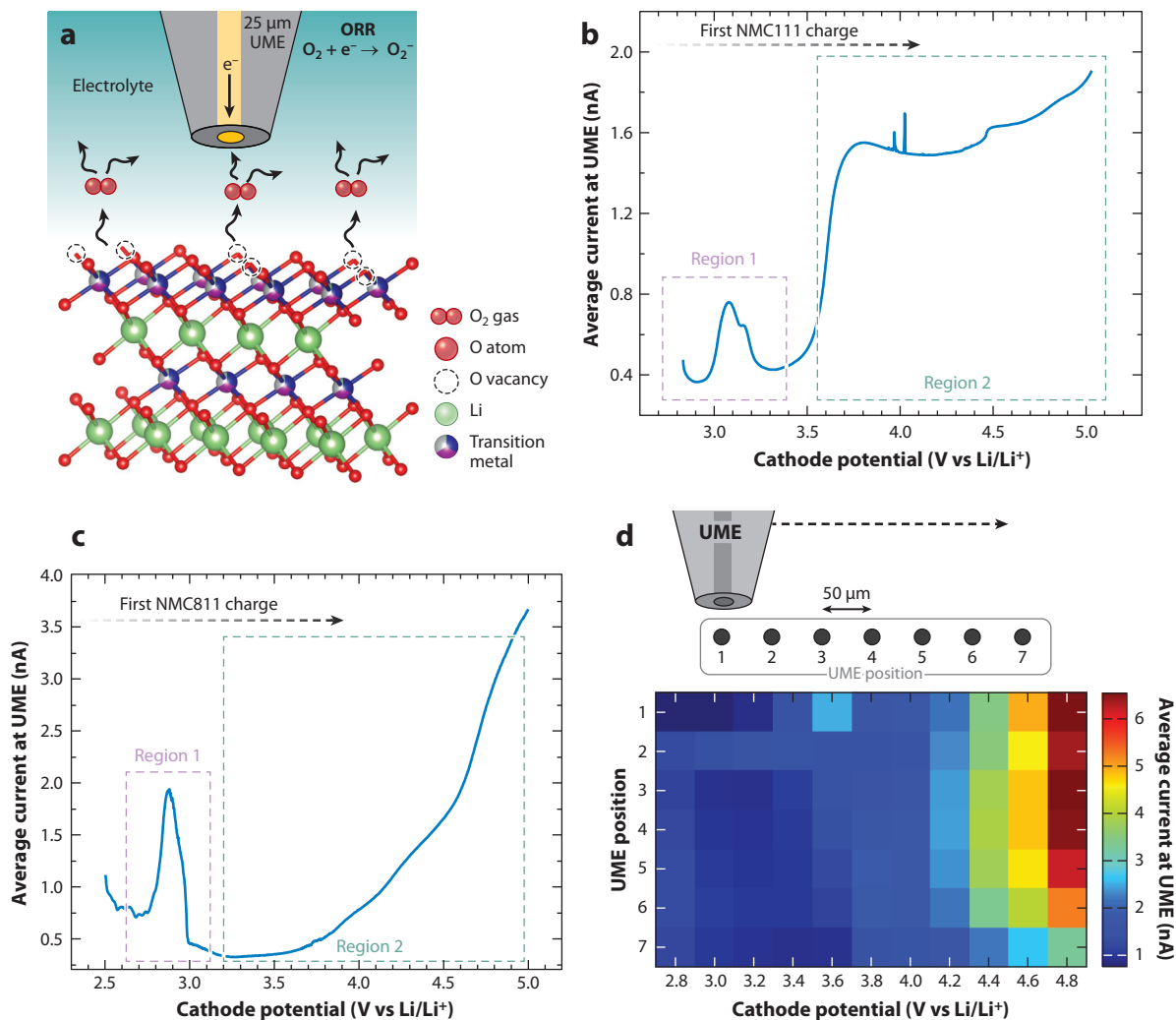


**Figure 4**

In situ investigation of oxygen evolution from Li-ion battery cathode materials using SECM. (a) Schematic of the experimental setup for real-time detection of lattice oxygen loss using SECM. Experimental data detailing lattice oxygen loss characteristics during the first charge cycle from (b) NMC111 and (c) NMC811, showing a previously unreported oxygen evolution event (Region 1) in addition to the main oxygen evolution process (Region 2). (d) SECM mapping experiments for investigating spatial heterogeneity in oxygen evolution from NMC111, as evidenced by the differences in oxygen evolution profiles at the different locations. Abbreviations: NMC111,  $LiNi_{0.33}Mn_{0.33}Co_{0.33}O_2$ ; NMC811,  $LiNi_{0.8}Mn_{0.1}Co_{0.1}O_2$ ; ORR, oxygen reduction reaction; SECM, scanning electrochemical microscopy; UME, ultramicroelectrode. Figure adapted with permission from Reference 28; copyright 2022 IOP Publishing.

media (67, 70, 71, 81, 83), ionic liquids (84), and nonvolatile carbonate solvents (62, 69). While EC-AFM and SECM measurements have been reported in gloveboxes, SECCM performance within a glovebox has been benchmarked recently with relevant carbonate solvents (85). Usage of volatile solvents such as dimethylcarbonate led to irreproducible SECCM responses over time, and salt precipitation on the substrate was observed postexperiment (85). There is a need and opportunity to solve these issues associated with ESPTs for obtaining practically relevant information that impacts real-world batteries.

## 4. APPLICATION OF ESPTs TO ALTERNATIVE BATTERY CHEMISTRIES

Alternative battery technologies to LiBs include chemistries such as Li-O<sub>2</sub> batteries and redox flow batteries (RFBs), among others. Li-O<sub>2</sub> batteries theoretically possess capacities of an order of magnitude greater than LiBs, with the cathode relying on the ORR and the oxygen evolution reaction (OER) (**Figure 1a**) for reversible energy storage (86). On the other hand, RFBs are attractive candidates for grid-level energy storage since their power and capacity characteristics are decoupled (1, 87). RFBs store energy in redox-active molecules (ROMs) dissolved in solution, with current-collector electrodes utilized for (dis)charge processes.

### 4.1. Li-O<sub>2</sub> Batteries

A key challenge preventing the commercialization of Li-O<sub>2</sub> batteries is the formation of insulating Li<sub>2</sub>O<sub>2</sub> during battery operation. Subsequently, this leads to two major issues: (a) gas-diffusion electrode pores are clogged, preventing O<sub>2</sub> transport for further ORR; and (b) the insulating Li<sub>2</sub>O<sub>2</sub> requires a large overpotential for OER, reducing the available energy during battery discharge. Schwager et al. (88) used in situ SECM to characterize the clogging problem by tracking oxygen flux in real time through collection measurements at the UME tip. SECM has also been used to identify homogeneous redox mediators for Li<sub>2</sub>O<sub>2</sub> oxidation through ex situ measurements (89, 90). Such examples enable identifying strategies to overcome energy losses incurred during Li<sub>2</sub>O<sub>2</sub> oxidation during the discharge of Li-O<sub>2</sub> batteries.

An alternative strategy to probe discharge processes in Li-O<sub>2</sub> batteries involves using in situ EC-AFM to study the oxidation of Li<sub>2</sub>O<sub>2</sub> films on different substrates such as HOPG, glassy carbon, and nanoporous gold electrodes (91–93). One such study also revealed that ORR products decomposed at potentials more positive than 4.4 V versus Li<sup>+</sup>/Li during discharge (94). In the same study, additional mechanistic details such as reaction intermediates and final products were obtained by combining EC-AFM with infrared spectroscopy and surface-enhanced Raman spectroscopy. In situ EC-AFM is a promising tool for visualizing the changes during Li-O<sub>2</sub> battery operation, which is required for elucidating the catalytic processes occurring at these cathodes.

### 4.2. Redox Flow Batteries

The fundamental process in RFBs is the ET from the electrode to ROMs in solution (13). SECM feedback mode is a powerful tool to apply in RFB characterization since feedback measurements quantify ET rates from a substrate electrode to a redox-active mediator in solution. Such quantitative measurements of ET kinetics have been previously reported through SECM approach curve measurements in nonaqueous RFB systems (95, 96). SECM and EC-AFM have also been applied in situ to characterize the electrochemical reactivity of graphitic carbon electrodes toward practically relevant ROMs for nonaqueous RFBs (97). These measurements enabled the identification of metastable film formation (**Figure 5a**), occurring during the reduction process of dialkoxybenzene ROM (98) on HOPG. Correlative measurements with SECM highlighted low electrochemical reactivity (**Figure 5b**) and passivation (**Figure 5c**) associated with the conditions leading to film formation. It was also revealed that ET rates showed little dependence on applied potential (**Figure 5d**). This study additionally reported that carbon electrode structure (edge planes versus basal planes) and choice of supporting electrolyte can partially mitigate limitations in ET kinetics. This example highlights how SECM and EC-AFM can be used in tandem to characterize and mitigate fundamental issues regarding ET processes in RFBs.

Downloaded from www.annualreviews.org.

Guest (guest)

www.annualreviews.org • Imaging of Interfaces in Energy Storage 105

On: Thu, 16 May 2024 16:04:41

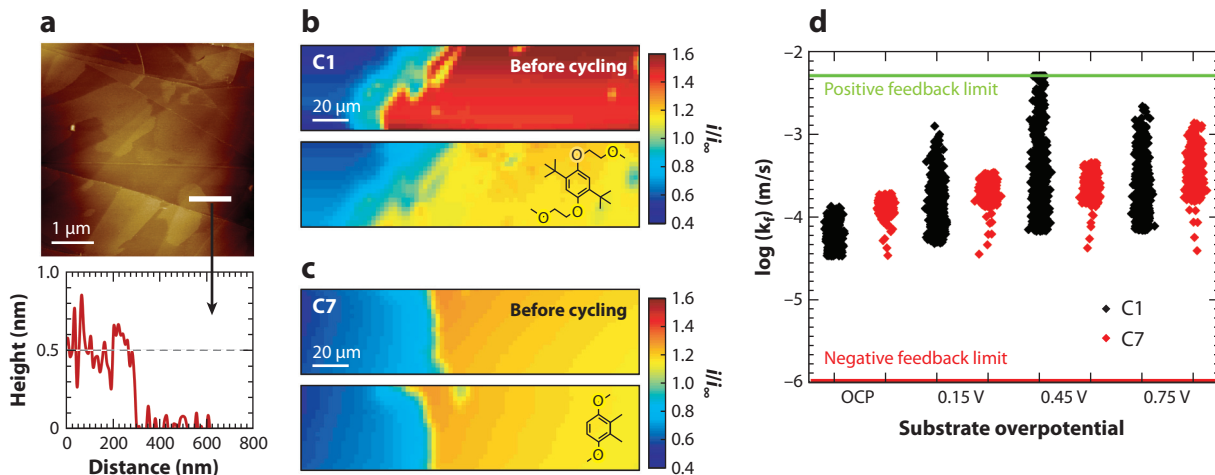


**Figure 5**

Application of in situ electrochemical atomic force microscopy (EC-AFM) and scanning electrochemical microscopy (SECM) to characterize electron transfer and film formation on graphitic carbon electrodes for redox flow batteries. (a) AFM topographical image (top) illustrating the formation of films  $\sim 0.5$  nm in thickness (bottom) on basal planes of highly oriented pyrolytic graphite. The white line indicates the position where the height profile is taken for the figure below, as indicated by the black arrow. SECM feedback images before (top) and after (bottom) cycling reveal (b) deterioration in electron transfer (ET) kinetics and (c) low ET kinetics for dialkoxybenzene redox-active molecules (C1 and C7), respectively. Structures are shown as insets. (d) Analysis of ET rate constants ( $k_f$ ) versus applied overpotentials at the substrate illustrates low/no influence of applied potential, in contrast to the Butler-Volmer kinetics model. Green and red lines denote mass-transfer limits for measurable  $k_f$  values. Figure adapted with permission from Reference 97; copyright 2020 Royal Society of Chemistry.

### 4.3. Applications to Other EESSs

In addition to the above-mentioned battery chemistries, ESPTs have been applied to other emerging EESSs as well. For example, feedback and ion-sensitive imaging using SECM was recently utilized to study the incipient SEI formed by  $\text{Li}^+$ ,  $\text{Na}^+$ , and  $\text{K}^+$  on multilayer graphene for insight into Na-ion and K-ion systems (64). The study concluded that a SEI based on Li electrolytes had the highest passivation and cation influx and correlated these observations to the presence of higher fluoride content in the SEI. Operando EC-AFM has also been utilized creatively to elucidate the energy storage mechanism of proton intercalation in  $\text{WO}_3$  by tracking its associated deformation (99). **Figure 6a,b** shows surface morphology of the  $\text{WO}_3$  and  $\text{WO}_3 \cdot 2\text{H}_2\text{O}$  samples used in the study. **Figure 6c,e** and **Figure 6d,f** show the spatial variation in local deformation rate at the cathodic peak current potential and at the anodic peak current potential, respectively. A higher, nonuniform deformation takes place in  $\text{WO}_3$  as compared to  $\text{WO}_3 \cdot 2\text{H}_2\text{O}$ , thereby highlighting the role of confined structural water on the mechanical response to proton insertion. Another major point concluded from these measurements was that for high-rate capabilities, the material must have a flexible structure, in addition to high electronic and ionic conductivity, in order to accommodate the structural changes during charge storage.

## 5. PERSPECTIVES ON HARDWARE AND SOFTWARE METHODS TO ADVANCE ESPTs

While ESPTs offer critical information on interfacial processes occurring in EESSs, the spatial resolution offered by these techniques does not match contemporary ex situ techniques. Also, many electrodes used in EESSs present complex morphologies that complicate the performance

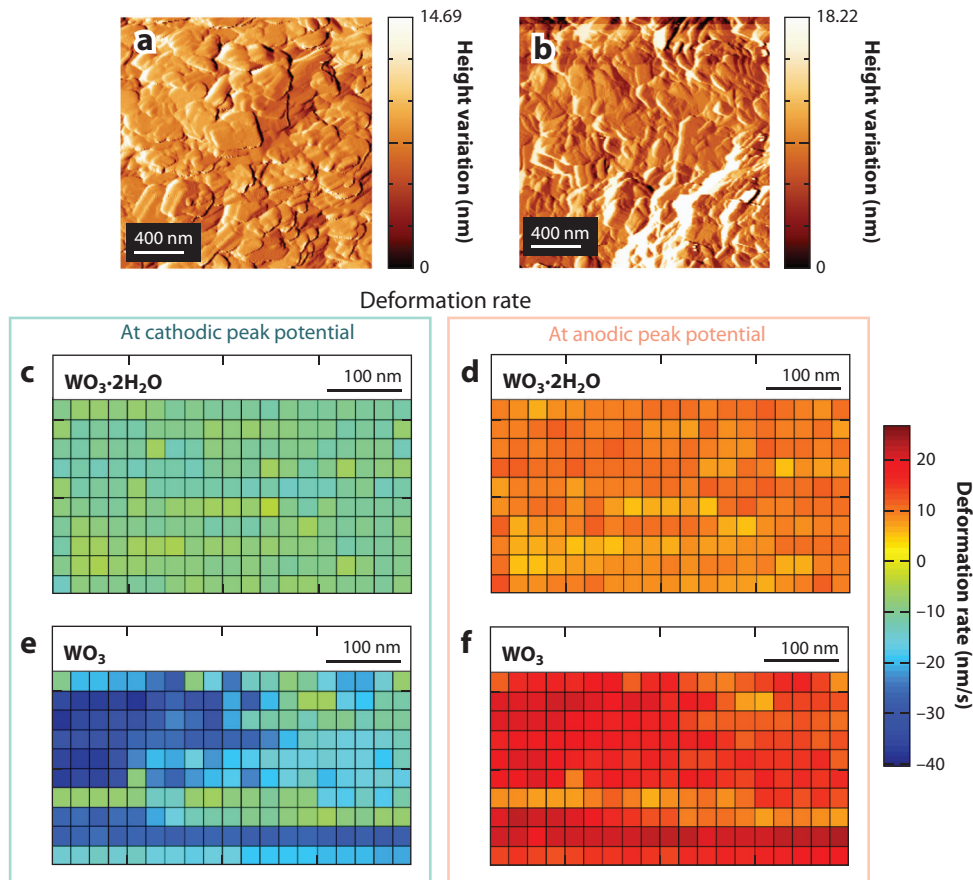


**Figure 6**

Investigation of proton insertion inside  $\text{WO}_3$  and  $\text{WO}_3 \cdot 2\text{H}_2\text{O}$  using operando electrochemical atomic force microscopy. Surface morphology is shown for (a)  $\text{WO}_3$  and (b)  $\text{WO}_3 \cdot 2\text{H}_2\text{O}$ . Spatial variations of the local deformation rates at the (c,e) cathodic peak current potentials and (d,f) anodic peak current potentials are shown. The distance between each grid point in panels c–f is 25 nm. Figure adapted with permission from Reference 99; copyright 2018 American Chemical Society.

of tip-based measurements. The possible solutions include not just advancements in hardware but also the incorporation of novel computational tools in ESPT studies. Another area of advancement lies in automating ESPT measurements to enable high-throughput studies for rapid investigation of battery processes. A perspective on these approaches is provided below.

### 5.1. Improving Imaging Resolution

An issue that is inherent to SECM is the convolution of electrochemical and morphological information. Sharp features such as boundaries between two dissimilar regions are difficult to resolve due to the diffusional broadening of redox mediators, which is sensitive to the tip-substrate distance and the tip geometry. While resolution could be improved by using smaller tip sizes, the fabrication of nanometer-sized electrodes often requires high skill and specialized equipment (100, 101). Different strategies have been used to address this issue of resolving topographical features. One approach involves performing correlative microscopy measurements of

### Deep learning:

an artificial intelligent algorithm where a computer learns from experience using a complicated hierarchy of simple concepts

morphology and electrochemical properties from the same/similar sample. In this regard, SICM could be employed for measuring topography since it has a better resolution than SECM, being limited only by the diameter of the pipette and the distance to the substrate (21). Additionally, its operation does not require a redox mediator. To ensure interrogation of the same region, some groups have been using multifunctional probes, for example, multifunctional AFM-SECM (102) and SICM-SECM (30, 34, 103–105) tips.

Further improvements beyond the hardware solutions discussed above will require postprocessing data to deconvolute morphological and electrochemical information as well as to improve image quality. Resolution enhancement of SEM images with deep learning methods has been demonstrated by de Haan et al. (106) and enables obtaining low-resolution images followed by postprocessing to increase image resolution, as illustrated in **Figure 7a**. Such approaches are starting to find their way into ESPT applications, for example, edge-detection algorithms have been applied to SECM by Stephens et al. (107). In their work, they show that the inflection point in a sigmoidal current profile curve strongly indicates the presence of a feature edge. They used this information to obtain SECM images of patterned substrates and compared them with electron microscopy images, allowing them to accurately estimate feature size. This methodology, however, still has limitations; it works best when a high-contrast image with a high density of points is obtained and when the size of the feature is larger than the UME. Likewise, current profiles exhibiting nonuniform feedback behavior can show multiple inflection points not precisely related to a morphological feature. Subsequently, they implemented an algorithm based on a point spread function to increase the resolution of SECM images without the need of decreasing the tip size (107). Their approach allowed dramatic improvement in the SECM image quality of patterned Au/SiO<sub>2</sub> samples, as shown in **Figure 7b**. This methodology, however, is computationally expensive and requires additional expertise to extract more quantitative information. However, these examples clearly illustrate that data postprocessing and simulation-based methodologies are a viable path to follow to make SECM resolutions compete with other imaging techniques (108).

## 5.2. Enabling Automation in ESPTs

The scanning probe microscopy (SPM) community has been working on implementing searching and artificial intelligence algorithms to automate feature identification (111, 112). In SECM applications, Balla et al. (109) have demonstrated that real-time analysis of approach curves with nanoscale tip–substrate distances can help resolve step edges of about 500 nm in height, as shown in **Figure 7c**. They developed an algorithm and software that enabled accurate tip positioning without the tip crashing into the substrate. Continuous progress on high-resolution ESPTs will open up new possibilities of studying the electrochemical reactivity of even smaller features. For example, deep learning has been used to analyze microscopy images for the automatic identification of particle properties, crystallographic features, and even atomic structures (110, 113–115). Krull et al. (110) developed DeepSPM, a software that automates scanning tunneling microscopy operation. The software automatically locates specific sample regions and tests the condition of the tip to ensure that the feature is not a tip artifact. It then decides whether the image is of an acceptable quality and can proceed to a different region or whether it should correct for tip problems. The full diagram of operation for this technology is shown in **Figure 7d**. This makes the acquisition of large data sets more feasible and opens the possibility of implementing nanolithography. The source of DeepSPM is publicly available, allowing other researchers to modify it according to their needs. The authors even suggest that the software can be generalized to any SPM technique. However, this not only requires advanced programming skills but will also require developers, for example, companies, to provide open-source frameworks that facilitate the communication between various instruments and tools such as DeepSPM.

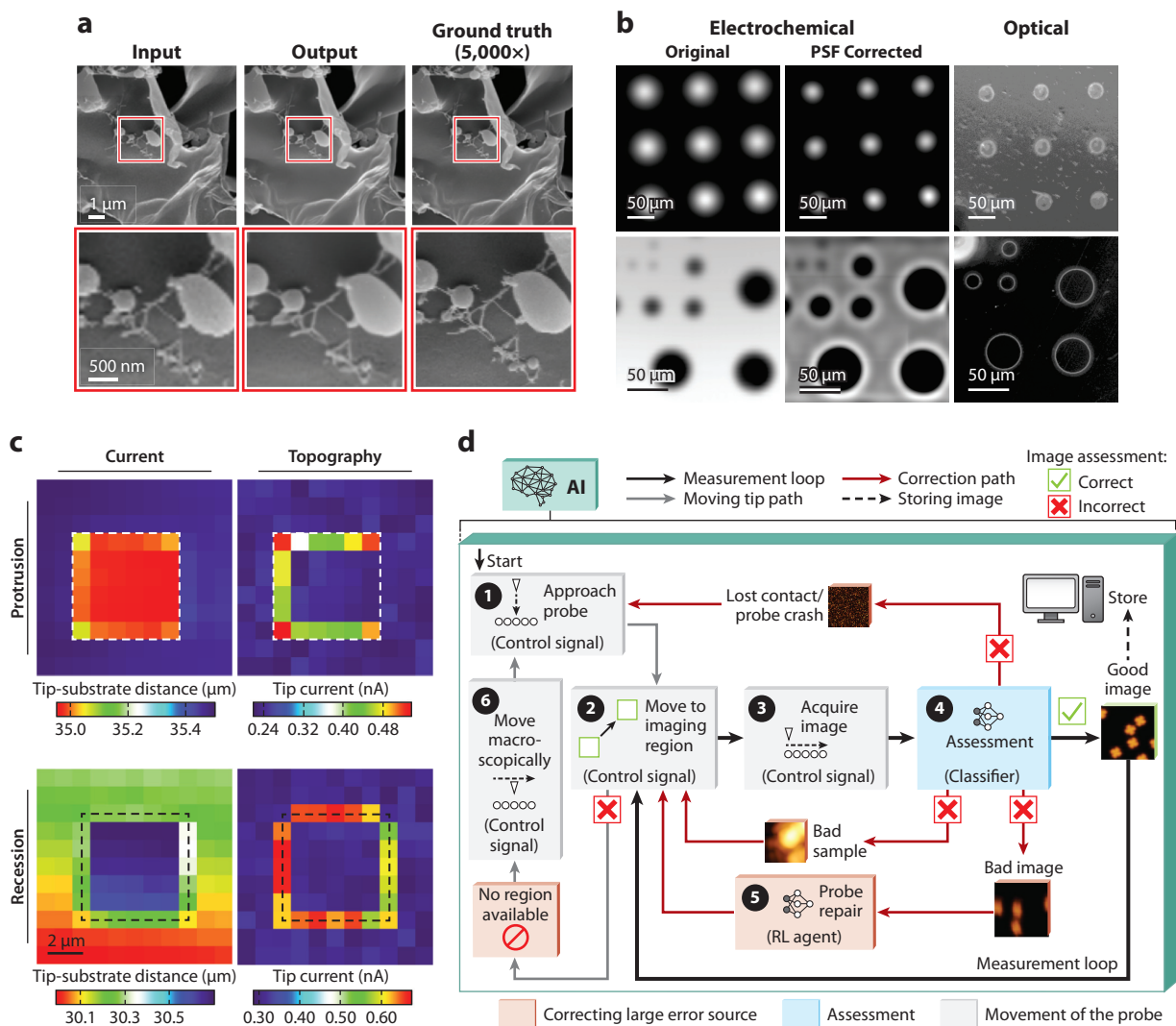


**Figure 7**

Perspectives on the improvement of electrochemical scanning probe techniques. (a) Resolution enhancement of hydrogels by deep learning, showing the input, output, and real (ground truth) images. Panel a adapted with permission from Reference 106; copyright 2019 Springer Nature. (b) Resolution enhancement of scanning electrochemical microscopy (SECM) images with the point spread function (PSF)-based deconvolution, where the white and black colors represent conductive and nonconductive regions, respectively. Examples are for two different geometries (*top* and *bottom*). Panel b adapted with permission from Reference 107; copyright 2020 American Chemical Society. (c) Edge detection using the real-time analysis of SECM approach curves: topography (*right*) and current (*left*) at a protrusion (*top*) and recession (*bottom*) on insulating substrates in 10-mM  $\text{Ru}(\text{NH}_3)_6^{3+}$  and 1-M KCl. The edges are represented by dashed boxes. Panel c adapted with permission from Reference 109; copyright 2019 American Chemical Society. (d) Workflow of the DeepSPM software, showing the approach curve, finding of an area, decision-making to test the quality of the image, and correction by repairing the probe and moving to a new region. Panel d adapted with permission from Reference 110; copyright 2020 Springer Nature.

## 6. CONCLUDING REMARKS

ESPTs are uniquely positioned to investigate interfacial processes occurring during operation of electrodes for EESSs. The examples discussed here illustrate their high versatility and ability to operate in situ with minimal damage or influence on electrode operation. However, there is significant room for improvement on ESPTs applied to EESSs: First, ESPTs are utilized extensively to characterize LiB electrode materials, but they are not yet widely used in the characterization of other structural battery components such as separators or current collectors. Second, they have also been underutilized to probe emerging battery chemistries such as RFBs and solid-state batteries. We foresee that multimodal techniques combining ESPTs with spectroscopic, spectrometric, and electron- or X-ray-based methods will significantly elevate their diagnostic power (7). However, this will also require improving their spatial resolution and their versatility at interrogating relevant electrode morphologies. In this regard, improvements in ESPT hardware and software for data postprocessing and improving imaging quality might not be enough. Perhaps future applications will include advanced algorithms to identify and decide on the best course of action when encountering surface features or for matching the spot size of a complementary technique used alongside the ESPT. A final remark concerns the applicability of the in situ information generated by the ESPT with respect to its translation to the device level. Fundamental investigations inform new strategies to improve EESSs, but increasing the sophistication of imaging experiments will always be desirable for obtaining practical insights that are directly relevant to commercial batteries.

## DISCLOSURE STATEMENT

The authors are not aware of any affiliations, memberships, funding, or financial holdings that might be perceived as affecting the objectivity of this review.

## ACKNOWLEDGMENTS

The authors gratefully acknowledge financial support from National Science Foundation Division of Materials Research award 1905803 and from the Joint Center for Energy Storage Research, an Energy Innovation Hub funded by the US Department of Energy, Office of Science, Basic Energy Sciences. A.M. gratefully acknowledges support from the Link Foundation Energy Fellowship.

## LITERATURE CITED

1. Trahey L, Brushett FR, Balsara NP, Ceder G, Cheng L, et al. 2020. Energy storage emerging: a perspective from the Joint Center for Energy Storage Research. *PNAS* 117:12550–57
2. Whittingham S. 2014. Introduction: batteries. *Chem. Rev.* 114:11413
3. Wood DL, Li J, An SJ. 2019. Formation challenges of lithium-ion battery manufacturing. *Joule* 3:2884–88
4. López I, Morey J, Ledeuil JB, Madec L, Martinez H. 2021. A critical discussion on the analysis of buried interfaces in Li solid-state batteries. *Ex situ* and *in situ/operando* studies. *J. Mater. Chem. A* 9:25341–68
5. Gossage ZT, Schorr NB, Hernández-Burgos K, Hui J, Simpson BH, et al. 2017. Interrogating charge storage on redox active colloids via combined Raman spectroscopy and scanning electrochemical microscopy. *Langmuir* 33:9455–63
6. Schorr NB, Jiang AG, Rodríguez-López J. 2018. Probing graphene interfacial reactivity via simultaneous and colocalized Raman–scanning electrochemical microscopy imaging and interrogation. *Anal. Chem.* 90:7848–54
7. Schorr NB, Gossage ZT, Rodríguez-López J. 2018. Prospects for single-site interrogation using in situ multimodal electrochemical scanning probe techniques. *Curr. Opin. Electrochem.* 8:89–95

8. Ren Z, Mastropietro F, Davydok A, Langlais S, Richard M-I, et al. 2014. Scanning force microscope for in situ nanofocused X-ray diffraction studies. *J. Synchrotron Radiat.* 21:1128–33
9. Slobodskyy T, Zozulya AV, Tholapi R, Liefelth L, Fester M, et al. 2015. Versatile atomic force microscopy setup combined with micro-focused X-ray beam. *Rev. Sci. Instrum.* 86:065104
10. Hui J, Gossage ZT, Sarbapalli D, Hernández-Burgos K, Rodríguez-López J. 2019. Advanced electrochemical analysis for energy storage interfaces. *Anal. Chem.* 91:60–83
11. Bentley CL, Edmondson J, Meloni GN, Perry D, Shkirskiy V, Unwin PR. 2019. Nanoscale electrochemical mapping. *Anal. Chem.* 91:84–108
12. Ventosa E. 2021. Why nanoelectrochemistry is necessary in battery research? *Curr. Opin. Electrochem.* 25:100635
13. Sarbapalli D, Mishra A, Hatfield KO, Gossage ZT, Rodríguez-López J. 2021. Scanning electrochemical microscopy: a versatile tool for inspecting the reactivity of battery electrodes. In *Batteries: Materials Principles and Characterization Methods*, ed. C Liao, pp. 9–1–44. Bristol, UK: IOP Publ.
14. Zhang Z, Said S, Smith K, Jervis R, Howard CA, et al. 2021. Characterizing batteries by in situ electrochemical atomic force microscopy: a critical review. *Adv. Energy Mater.* 11:2101518
15. Winter M, Barnett B, Xu K. 2018. Before Li ion batteries. *Chem. Rev.* 118:11433–56
16. Bard AJ, Mirkin MV. 2022. *Scanning Electrochemical Microscopy*. Boca Raton: Taylor & Francis
17. Wahab OJ, Kang M, Unwin PR. 2020. Scanning electrochemical cell microscopy: a natural technique for single entity electrochemistry. *Curr. Opin. Electrochem.* 22:120–28
18. Ebejer N, Güell AG, Lai SCS, McKelvey K, Snowden ME, Unwin PR. 2013. Scanning electrochemical cell microscopy: a versatile technique for nanoscale electrochemistry and functional imaging. *Annu. Rev. Anal. Chem.* 6:329–51
19. Bentley CL, Kang M, Unwin PR. 2017. Scanning electrochemical cell microscopy: new perspectives on electrode processes in action. *Curr. Opin. Electrochem.* 6:23–30
20. Zhou L, Zhou Y, Baker LA. 2014. Measuring ions with scanning ion conductance microscopy. *Electrochem. Soc. Interface* 23:47–52
21. Choi M-H, Leasor CW, Baker LA. 2021. Analytical applications of scanning ion conductance microscopy: measuring ions and electrons. In *Scanning Ion Conductance Microscopy*, ed. TE Schaffer, pp. 73–121. Berlin/Heidelberg: Springer
22. Zhang Z, Smith K, Jervis R, Shearing PR, Miller TS, Brett DJL. 2020. Operando electrochemical atomic force microscopy of solid–electrolyte interphase formation on graphite anodes: the evolution of SEI morphology and mechanical properties. *ACS Appl. Mater. Interfaces* 12:35132–41
23. von Cresce A, Russell SM, Baker DR, Gaskell KJ, Xu K. 2014. In situ and quantitative characterization of solid electrolyte interphases. *Nano Lett.* 14:1405–12
24. Liu T, Lin L, Bi X, Tian L, Yang K, et al. 2019. In situ quantification of interphasial chemistry in Li-ion battery. *Nat. Nanotechnol.* 14:50–56
25. Li N-W, Shi Y, Yin Y-X, Zeng X-X, Li J-Y, et al. 2018. A flexible solid electrolyte interphase layer for long-life lithium metal anodes. *Angew. Chem. Int. Ed.* 57:1505–9
26. Shen X, Li Y, Qian T, Liu J, Zhou J, et al. 2019. Lithium anode stable in air for low-cost fabrication of a dendrite-free lithium battery. *Nat. Commun.* 10:900
27. Forster RJ, Keyes TE. 2007. Ultramicroelectrodes. In *Handbook of Electrochemistry*, ed. CG Zoski, pp. 155–71. Amsterdam: Elsevier
28. Mishra A, Sarbapalli D, Hossain MS, Gossage ZT, Li Z, et al. 2022. Highly sensitive detection and mapping of incipient and steady-state oxygen evolution from operating Li-ion battery cathodes via scanning electrochemical microscopy. *J. Electrochem. Soc.* 169:086501
29. Hansma PK, Drake B, Marti O, Gould SAC, Prater CB. 1989. The scanning ion-conductance microscope. *Science* 243:641–43
30. Page A, Perry D, Unwin PR. 2017. Multifunctional scanning ion conductance microscopy. *Proc. R. Soc. A* 473:20160889
31. Lipson AL, Ginder RS, Hersam MC. 2011. Nanoscale in situ characterization of Li-ion battery electrochemistry via scanning ion conductance microscopy. *Adv. Mater.* 23:5613–17

32. Takahashi Y, Takamatsu D, Korchev YE, Fukuma T. 2022. Correlative analysis of ion concentration profile and surface nanoscale topography changes using operando scanning ion conductance microscopy. ChemRxiv. <https://doi.org/10.26434/chemrxiv-2022-2pr2j>
33. Lipson AL, Puntambekar K, Comstock DJ, Meng X, Geier ML, et al. 2014. Nanoscale investigation of solid electrolyte interphase inhibition on Li-ion battery MnO electrodes via atomic layer deposition of Al<sub>2</sub>O<sub>3</sub>. *Chem. Mater.* 26:935–40
34. Morris CA, Chen C-C, Baker LA. 2012. Transport of redox probes through single pores measured by scanning electrochemical-scanning ion conductance microscopy (SECM-SICM). *Analyst* 137:2933–38
35. Payne NA, Dawkins JIG, Schougaard SB, Mauzeroll J. 2019. Effect of substrate permeability on scanning ion conductance microscopy: uncertainty in tip–substrate separation and determination of ionic conductivity. *Anal. Chem.* 91:15718–25
36. Peled E, Menkin S. 2017. Review—SEI: past, present and future. *J. Electrochem. Soc.* 164:A1703–19
37. Zhang H, Liu H, Piper LFJ, Whittingham MS, Zhou G. 2022. Oxygen loss in layered oxide cathodes for Li-ion batteries: mechanisms, effects, and mitigation. *Chem. Rev.* 122:5641–81
38. Li W. 2020. Review—An unpredictable hazard in lithium-ion batteries from transition metal ions: dissolution from cathodes, deposition on anodes and elimination strategies. *J. Electrochem. Soc.* 167:090514
39. Asenbauer J, Eisenmann T, Kuenzel M, Kazzazi A, Chen Z, Bresser D. 2020. The success story of graphite as a lithium-ion anode material—fundamentals, remaining challenges, and recent developments including silicon (oxide) composites. *Sustain. Energy Fuels* 4:5387–416
40. Lin D, Liu Y, Cui Y. 2017. Reviving the lithium metal anode for high-energy batteries. *Nat. Nanotechnol.* 12:194–206
41. Bültner H, Peters F, Schwenzel J, Wittstock G. 2014. Spatiotemporal changes of the solid electrolyte interphase in lithium-ion batteries detected by scanning electrochemical microscopy. *Angew. Chem. Int. Ed.* 53:10531–35
42. Yamada Y, Miyazaki K, Abe T. 2010. Role of edge orientation in kinetics of electrochemical intercalation of lithium-ion at graphite. *Langmuir* 26:14990–94
43. Bültner H, Peters F, Wittstock G. 2016. Scanning electrochemical microscopy for the in situ characterization of solid–electrolyte interphases: highly oriented pyrolytic graphite versus graphite composite. *Energy Technol.* 4:1486–94
44. Hui J, Burgess M, Zhang J, Rodríguez-López J. 2016. Layer number dependence of Li<sup>+</sup> intercalation on few-layer graphene and electrochemical imaging of its solid–electrolyte interphase evolution. *ACS Nano* 10:4248–57
45. Zampardi G, Ventosa E, La Mantia F, Schuhmann W. 2013. In situ visualization of Li-ion intercalation and formation of the solid electrolyte interphase on TiO<sub>2</sub> based paste electrodes using scanning electrochemical microscopy. *Chem. Commun.* 49:9347–49
46. Tarnev T, Wilde P, Dopilka A, Schuhmann W, Chan CK, Ventosa E. 2020. Surface properties of battery materials elucidated using scanning electrochemical microscopy: the case of type I silicon clathrate. *ChemElectroChem* 7:665–71
47. Martín-Yerga D, Kang M, Unwin PR. 2021. Scanning electrochemical cell microscopy in a glovebox: structure–activity correlations in the early stages of solid–electrolyte interphase formation on graphite. *ChemElectroChem* 8:4240–51
48. Martín-Yerga D, Milan DC, Xu X, Fernández-Vidal J, Whalley L, et al. 2022. Dynamics of solid–electrolyte interphase formation on silicon electrodes revealed by combinatorial electrochemical screening. *Angew. Chem. Int. Ed.* 61:e202207184
49. Campana FP, Kötz R, Vetter J, Novák P, Siegenthaler H. 2005. In situ atomic force microscopy study of dimensional changes during Li<sup>+</sup> ion intercalation/de-intercalation in highly oriented pyrolytic graphite. *Electrochem. Commun.* 7:107–12
50. Alliaata D, Kötz R, Novák P, Siegenthaler H. 2000. Electrochemical SPM investigation of the solid electrolyte interphase film formed on HOPG electrodes. *Electrochem. Commun.* 2:436–40
51. Domi Y, Doi T, Yamanaka T, Abe T, Ogumi Z. 2013. Electrochemical AFM study of surface films formed on the HOPG edge plane in propylene carbonate-based electrolytes. *J. Electrochem. Soc.* 160:A678–83

Downloaded from [www.annualreviews.org](http://www.annualreviews.org).

Guest (guest)

IP: 18.223.118.70

On: Thu, 16 May 2024 16:04:41

52. Wang L, Deng D, Lev LC, Ng S. 2014. In-situ investigation of solid-electrolyte interphase formation on the anode of Li-ion batteries with atomic force microscopy. *J. Power Sources* 265:140–48
53. An SJ, Li J, Daniel C, Mohanty D, Nagpure S, Wood DL. 2016. The state of understanding of the lithium-ion-battery graphite solid electrolyte interphase (SEI) and its relationship to formation cycling. *Carbon* 105:52–76
54. Domi Y, Ochida M, Tsubouchi S, Nakagawa H, Yamanaka T, et al. 2012. Electrochemical AFM observation of the HOPG edge plane in ethylene carbonate-based electrolytes containing film-forming additives. *J. Electrochem. Soc.* 159:A1292–97
55. Matsuoka O, Hiwara A, Omi T, Toriida M, Hayashi T, et al. 2002. Ultra-thin passivating film induced by vinylene carbonate on highly oriented pyrolytic graphite negative electrode in lithium-ion cell. *J. Power Sources* 108:128–38
56. Yan J, Zhang J, Su Y-C, Zhang X-G, Xia B-J. 2010. A novel perspective on the formation of the solid electrolyte interphase on the graphite electrode for lithium-ion batteries. *Electrochim. Acta* 55:1785–94
57. Shen C, Hu G, Cheong L-Z, Huang S, Zhang J-G, Wang D. 2018. Direct observation of the growth of lithium dendrites on graphite anodes by operando EC-AFM. *Small Methods* 2:1700298
58. Tokranov A, Kumar R, Li C, Minne S, Xiao X, Sheldon BW. 2016. Control and optimization of the electrochemical and mechanical properties of the solid electrolyte interphase on silicon electrodes in lithium ion batteries. *Adv. Energy Mater.* 6:1502302
59. Beaulieu LY, Hatchard TD, Bonakdarpour A, Fleischauer MD, Dahn JR. 2003. Reaction of Li with alloy thin films studied by in situ AFM. *J. Electrochem. Soc.* 150:A1457
60. Becker CR, Strawhecker KE, McAllister QP, Lundgren CA. 2013. In situ atomic force microscopy of lithiation and delithiation of silicon nanostructures for lithium ion batteries. *ACS Nano* 7:9173–82
61. Krueger B, Balboa L, Dohmann JF, Winter M, Bieker P, Wittstock G. 2020. Solid electrolyte interphase evolution on lithium metal electrodes followed by scanning electrochemical microscopy under realistic battery cycling current densities. *ChemElectroChem* 7:3590–96
62. Gossage ZT, Hui J, Zeng Y, Flores-Zuleta H, Rodríguez-López J. 2019. Probing the reversibility and kinetics of Li<sup>+</sup> during SEI formation and (de)intercalation on edge plane graphite using ion-sensitive scanning electrochemical microscopy. *Chem. Sci.* 10:10749–54
63. Gossage ZT, Hui J, Sarbapalli D, Rodríguez-López J. 2020. Coordinated mapping of Li<sup>+</sup> flux and electron transfer reactivity during solid-electrolyte interphase formation at a graphene electrode. *Analyst* 145:2631–38
64. Zeng Y, Gossage ZT, Sarbapalli D, Hui J, Rodríguez-López J. 2022. Tracking passivation and cation flux at incipient solid-electrolyte interphases on multi-layer graphene using high resolution scanning electrochemical microscopy. *ChemElectroChem* 9:e202101445
65. Manthiram A. 2020. A reflection on lithium-ion battery cathode chemistry. *Nat. Commun.* 11:1550
66. Zhang Y, Yang Z, Tian C. 2019. Probing and quantifying cathode charge heterogeneity in Li ion batteries. *J. Mater. Chem. A* 7:23628–61
67. Takahashi Y, Kumatani A, Munakata H, Inomata H, Ito K, et al. 2014. Nanoscale visualization of redox activity at lithium-ion battery cathodes. *Nat. Commun.* 5:5450
68. Takahashi Y, Yamashita T, Takamatsu D, Kumatani A, Fukuma T. 2020. Nanoscale kinetic imaging of lithium ion secondary battery materials using scanning electrochemical cell microscopy. *Chem. Commun.* 56:9324–27
69. Snowden ME, Dayeh M, Payne NA, Gervais S, Mauzeroll J, Schougaard SB. 2016. Measurement on isolated lithium iron phosphate particles reveals heterogeneity in material properties distribution. *J. Power Sources* 325:682–89
70. Tao B, Yule LC, Daviddi E, Bentley CL, Unwin PR. 2019. Correlative electrochemical microscopy of Li-ion (de)intercalation at a series of individual LiMn<sub>2</sub>O<sub>4</sub> particles. *Angew. Chem. Int. Ed.* 58:4606–11
71. Inomata H, Takahashi Y, Takamatsu D, Kumatani A, Ida H, et al. 2019. Visualization of inhomogeneous current distribution on ZrO<sub>2</sub>-coated LiCoO<sub>2</sub> thin-film electrodes using scanning electrochemical cell microscopy. *Chem. Commun.* 55:545–48
72. Zhu X, Ong CS, Xu X, Hu B, Shang J, et al. 2013. Direct observation of lithium-ion transport under an electrical field in Li<sub>x</sub>CoO<sub>2</sub> nanograins. *Sci. Rep.* 3:1084

73. Sharifi-Asl S, Lu J, Amine K, Shahbazian-Yassar R. 2019. Oxygen release degradation in Li-ion battery cathode materials: mechanisms and mitigating approaches. *Adv. Energy Mater.* 9:1900551
74. Wang H, Rus E, Sakuraba T, Kikuchi J, Kiya Y, Abruña HD. 2014. CO<sub>2</sub> and O<sub>2</sub> evolution at high voltage cathode materials of Li-ion batteries: a differential electrochemical mass spectrometry study. *Anal. Chem.* 86:6197–201
75. La Mantia F, Rosciano F, Tran N, Novák P. 2008. Direct evidence of oxygen evolution from Li<sub>1+x</sub>(Ni<sub>1/3</sub>Mn<sub>1/3</sub>Co<sub>1/3</sub>)<sub>1-x</sub>O<sub>2</sub> at high potentials. *J. Appl. Electrochem.* 38:893–96
76. Papp JK, Li N, Kaufman LA, Naylor AJ, Younesi R, et al. 2021. A comparison of high voltage outgassing of LiCoO<sub>2</sub>, LiNiO<sub>2</sub>, and Li<sub>2</sub>MnO<sub>3</sub> layered Li-ion cathode materials. *Electrochim. Acta* 368:137505
77. Xu C, Märker K, Lee J, Mahadevegowda A, Reeves PJ, et al. 2021. Bulk fatigue induced by surface reconstruction in layered Ni-rich cathodes for Li-ion batteries. *Nat. Mater.* 20:84–92
78. Huang D, Engtrakul C, Nanayakkara S, Mulder DW, Han S-D, et al. 2021. Understanding degradation at the lithium-ion battery cathode/electrolyte interface: connecting transition-metal dissolution mechanisms to electrolyte composition. *ACS Appl. Mater. Interfaces* 13:11930–39
79. Scipioni R, Isheim D, Barnett SA. 2020. Revealing the complex layered-mosaic structure of the cathode electrolyte interphase in Li-ion batteries. *Appl. Mater. Today* 20:100748
80. Lu W, Zhang J, Xu J, Wu X, Chen L. 2017. In situ visualized cathode electrolyte interphase on LiCoO<sub>2</sub> in high voltage cycling. *ACS Appl. Mater. Interfaces* 9:19313–18
81. Liu S, Liu D, Wang S, Cai X, Qian K, et al. 2019. Understanding the cathode electrolyte interface formation in aqueous electrolyte by scanning electrochemical microscopy. *J. Mater. Chem. A* 7:12993–96
82. Zampardi G, Trocoli R, Schuhmann W, La Mantia F. 2017. Revealing the electronic character of the positive electrode/electrolyte interface in lithium-ion batteries. *Phys. Chem. Chem. Phys.* 19:28381–87
83. Kumatani A, Takahashi Y, Miura C, Ida H, Inomata H, et al. 2019. Scanning electrochemical cell microscopy for visualization and local electrochemical activities of lithium-ion (de) intercalation process in lithium-ion batteries electrodes. *Surf. Interface Anal.* 51:27–30
84. Dayeh M, Ghavidel MRZ, Mauzeroll J, Schougaard SB. 2019. Micropipette contact method to investigate high-energy cathode materials by using an ionic liquid. *ChemElectroChem* 6:195–201
85. Bentley CL, Kang M, Unwin PR. 2020. Scanning electrochemical cell microscopy (SECCM) in aprotic solvents: practical considerations and applications. *Anal. Chem.* 92:11673–80
86. Kwak W-J, Rosy S, Sharon D, Xia C, Kim H, et al. 2020. Lithium–oxygen batteries and related systems: potential, status, and future. *Chem. Rev.* 120:6626–83
87. Sánchez-Díez E, Ventosa E, Guarnieri M, Trovò A, Flox C, et al. 2021. Redox flow batteries: status and perspective towards sustainable stationary energy storage. *J. Power Sources* 481:228804
88. Schwager P, Fenske D, Wittstock G. 2015. Scanning electrochemical microscopy of oxygen permeation through air-electrodes in lithium–air batteries. *J. Electroanal. Chem.* 740:82–87
89. Torres WR, Herrera SE, Tesio AY, del Pozo M, Calvo EJ. 2015. Soluble TTF catalyst for the oxidation of cathode products in Li-oxygen battery: a chemical scavenger. *Electrochim. Acta* 182:1118–23
90. Chen Y, Gao X, Johnson LR, Bruce PG. 2018. Kinetics of lithium peroxide oxidation by redox mediators and consequences for the lithium–oxygen cell. *Nat. Commun.* 9:767
91. Wen R, Hong M, Byon HR. 2013. In situ AFM imaging of Li–O<sub>2</sub> electrochemical reaction on highly oriented pyrolytic graphite with ether-based electrolyte. *J. Am. Chem. Soc.* 135:10870–76
92. Virwani K, Ansari Y, Nguyen K, Moreno-Ortiz FJA, Kim J, et al. 2019. In situ AFM visualization of Li–O<sub>2</sub> battery discharge products during redox cycling in an atmospherically controlled sample cell. *Beilstein J. Nanotechnol.* 10:930–40
93. Wen R, Byon HR. 2014. In situ monitoring of the Li–O<sub>2</sub> electrochemical reaction on nanoporous gold using electrochemical AFM. *Chem. Commun.* 50:2628–31
94. Liu C, Ye S. 2016. In situ atomic force microscopy (AFM) study of oxygen reduction reaction on a gold electrode surface in a dimethyl sulfoxide (DMSO)-based electrolyte solution. *J. Phys. Chem. C* 120:25246–55
95. Baran MJ, Braten MN, Montoto EC, Gossage ZT, Ma L, et al. 2018. Designing redox-active oligomers for crossover-free, nonaqueous redox-flow batteries with high volumetric energy density. *Chem. Mater.* 30:3861–66

Downloaded from www.annualreviews.org.

Guest (guest)

IP: 18.223.118.70

On: Thu, 16 May 2024 16:04:41

96. Burgess M, Chénard E, Hernández-Burgos K, Nagarjuna G, Assary RS, et al. 2016. Impact of backbone tether length and structure on the electrochemical performance of viologen redox active polymers. *Chem. Mater.* 28:7362–74
97. Watkins TS, Sarbapalli D, Counihan MJ, Danis AS, Zhang J, et al. 2020. A combined SECM and electrochemical AFM approach to probe interfacial processes affecting molecular reactivity at redox flow battery electrodes. *J. Mater. Chem. A* 8:15734–45
98. Huang J, Pan B, Duan W, Wei X, Assary RS, et al. 2016. The lightest organic radical cation for charge storage in redox flow batteries. *Sci. Rep.* 6:32102
99. Wang R, Mitchell JB, Gao Q, Tsai W-Y, Boyd S, et al. 2018. Operando atomic force microscopy reveals mechanics of structural water driven battery-to-pseudocapacitor transition. *ACS Nano* 12:6032–39
100. Wang X, Han L, Xin H, Mirkin MV. 2019. TEM-assisted fabrication of sub-10 nm scanning electrochemical microscopy tips. *Anal. Chem.* 91:15355–59
101. Kai T, Zoski CG, Bard AJ. 2018. Scanning electrochemical microscopy at the nanometer level. *Chem. Commun.* 54:1934–47
102. Shi X, Qing W, Marhaba T, Zhang W. 2020. Atomic force microscopy-scanning electrochemical microscopy (AFM-SECM) for nanoscale topographical and electrochemical characterization: principles, applications and perspectives. *Electrochim. Acta* 332:135472
103. Takahashi Y, Shevchuk AI, Novak P, Murakami Y, Shiku H, et al. 2010. Simultaneous noncontact topography and electrochemical imaging by SECM/SICM featuring ion current feedback regulation. *J. Am. Chem. Soc.* 132:10118–26
104. Pollard AJ, Faruqui N, Shaw M, Clifford CA, Takahashi Y, et al. 2012. Development of a novel combined scanning electrochemical microscope (SECM) and scanning ion-conductance microscope (SICM) probe for soft sample imaging. *MRS Proc.* 1422:13–18
105. Comstock DJ, Elam JW, Pellin MJ, Hersam MC. 2010. Integrated ultramicroelectrode–nanopipet probe for concurrent scanning electrochemical microscopy and scanning ion conductance microscopy. *Anal. Chem.* 82:1270–76
106. de Haan K, Ballard ZS, Rivenson Y, Wu Y, Ozcan A. 2019. Resolution enhancement in scanning electron microscopy using deep learning. *Sci. Rep.* 9:12050
107. Stephens LL, Payne NA, Mauzeroll J. 2020. Super-resolution scanning electrochemical microscopy. *Anal. Chem.* 92:3958–63
108. Unwin P. 2022. Concluding remarks: next generation nanoelectrochemistry—next generation nanoelectrochemists. *Faraday Discuss.* 233:374–91
109. Balla RJ, Jantz DT, Kurapati N, Chen R, Leonard KC, Amemiya S. 2019. Nanoscale intelligent imaging based on real-time analysis of approach curve by scanning electrochemical microscopy. *Anal. Chem.* 91:10227–35
110. Krull A, Hirsch P, Rother C, Schiffrin A, Krull C. 2020. Artificial-intelligence-driven scanning probe microscopy. *Commun. Phys.* 3:54
111. Sotres J, Boyd H, Gonzalez-Martinez JF. 2021. Enabling autonomous scanning probe microscopy imaging of single molecules with deep learning. *Nanoscale* 13:9193–203
112. Ziatdinov M, Liu Y, Kelley K, Vasudevan R, Kalinin SV. 2022. Bayesian active learning for scanning probe microscopy: from Gaussian processes to hypothesis learning. *ACS Nano* 16:13492–512
113. Ziatdinov M, Dyck O, Maksov A, Li X, Sang X, et al. 2017. Deep learning of atomically resolved scanning transmission electron microscopy images: chemical identification and tracking local transformations. *ACS Nano* 11:12742–52
114. Okunev AG, Mashukov MY, Nartova AV, Matveev AV. 2020. Nanoparticle recognition on scanning probe microscopy images using computer vision and deep learning. *Nanomaterial* 10:1285
115. Ge M, Su F, Zhao Z, Su D. 2020. Deep learning analysis on microscopic imaging in materials science. *Mater. Today Nano* 11:100087